Journal of Applied Fluid Mechanics, Vol. 12, No. 5, pp. 1585-1597, 2019.
Available online at www.jafmonline.net, ISSN 1735-3572, EISSN 1735-3645.
DOI: 10.29252/jafm.12.05.29637

Computational Fluid Dynamics Simulation on Particulate Distribution in Gyro Casting for the Manufacture of Al/SiC Particulate Metal Matrix Composite

P. A. Abdul Samad[1†], P. R. Shalij[2], A. Ramesh[1] and A. K. Mubarak[1]

[1.] *Department of Mechanical Engineering, Government Engineering College, Thrissur, Kerala, PIN:680009, India*

[2.] *Department of Production Engineering, Government Engineering College, Thrissur, Kerala, PIN:680009, India*

†*Corresponding Author Email:abdulsamad@gectcr.ac.in*

(Received September 12, 2018; accepted December 14, 2018)

ABSTRACT

The enhanced specific strength of SiC Particulate Metal Matrix Composites (PMMC) has been the major contributing factor which helps to find applications in the aerospace and automotive industries. Uniform distribution of the particulates in PMMC controls the attainment of better mechanical properties. The most accepted method for producing such a composite is stir casting in which the homogeneity of particulate reinforcement is a significant challenge. This research work proposes a new method for mixing the particulate reinforcement with the liquid and semi-solid aluminium matrix to ensure a uniform mix of the particulates using a gyro shaker. Gyro shaker is a dual rotation mixer commonly used for mixing high viscous fluids. It rotates about two mutually perpendicular axes which help in thoroughly mixing of the ingredients. Developed Computational Fluid Dynamics (CFD) simulation model of the mixing device in finding the mixing performance while mixing SiC particulates with glycerol. The results of the simulation were also validated by experimentation. Analogue fluid simulation of gyro casting was carried out using water and glycerol/water mixture which are having a closer value of viscosity as that of liquid aluminium and semi-solid aluminium. The mixing time obtained in the water system at gyration speeds of 29.63 rpm, 58.18 rpm, 72.73 rpm and 87.27 rpm was 61.84 sec, 43.44 sec, 26.85 sec and 27.24 sec respectively. The mixing time obtained in glycerol/water system at gyration speeds of 58.18 rpm, 87.27 rpm, 116.36 rpm and 145.45 rpm was 26.34 sec, 15.97 sec, 9.8 sec and 6.26 sec respectively. The distribution of the SiC particulates obtained from simulation was compared with stir casting simulations. The homogeneous distribution of particulates was observed in the gyro casting simulation.

Keywords: Gyro casting; Stir casting; Computational fluid dynamics; Mixing power; Grid independence study; Mixing index.

1. INTRODUCTION

Composites have a material configuration in which the reinforcement particulates are dispersed in continuous phase resulting in a combination of properties of the constituents. The combination properties of fluids can also modify by adding powdered metal oxides (Gupta *et al*., 2018a). The thermal performance of fluids can be improved by adding solid particles in nanometer size (Gupta *et al*., 2018b). Al-SiC PMMC is one of the widely used composites in the aerospace, sports and automotive due to its high specific strength. Materials like carbon nanotubes are also widely used as reinforcement due to its high tensile strength and modulus (Sharma, K *et al*., 2015). The most common method for the production of PMMC is stir casting. In stir casting, the molten metal is vigorously stirred using mechanical impeller while particulates are added for keeping the dispersed particle in suspension (Hashim *et al*., 1999).

Proper mixing of particulates in the production of PMMC and their distribution play a key role in determining the mechanical properties of the composite. The defects associated with the reinforcement while manufacturing will weaken the strength of the composite (Sharma *et al*., 2012). Prabu *et al*., (2006) conducted experiments and found that the mechanical properties are much influenced on the particulate distribution of the cast composite. Behera *et al*. (2012) conducted experiments for studying the distribution of SiC particulates in metal matrix composites made by stir casting and its effect on

mechanical properties. Yigezu *et al.* (2013) fabricated a hybrid composite using aluminium alloy as the matrix material and a mixture of SiC and Al2O3 powders as reinforcement using stir casting method. The microstructure study showed fairly distribution of Al2O3 and clustering of SiC particulates. Ghauri *et al.* (2013) tested mechanical properties and conducted a microscopic study to evaluate the clustering of particulates in the stir cast PMMC. The agglomeration of SiC particles resulted in lowering of properties regarding toughness and hardness. The centrifugal force of the larger particles causes the non-uniformity of particle distribution. Ezatpour *et al.* (2014) fabricated PMMC by stir casting with Al6061 aluminium alloy as the matrix material and SiC of 40nm size. The amount of SiCnano particulates varied from 0.5 to 1.5 wt%. The stir casting process followed by an extrusion process for producing the composite. He found agglomeration nanoparticles at higher wt% loading. Aigbodion (2014) manufactured particulate composite with ash powder and Al-Cu-Mg alloy by the stir casting method. The wt % of SiC is varied from 2 to 10. The microstructure analysis shows the agglomeration of ash particulates in the matrix. Sharma, P *et al.* (2015) made Aluminium matrix composites with graphite particulates by the stir casting process. The wt % of graphite is varied from 3 to 12. The microstructure of the cast PMMC shows a non-uniform distribution of graphite particulates. Kandpal *et al.* (2017) found clustering of Al_2O_3 particulates in the cast composite prepared by aluminium alloy 6061 as matrix material.

Numerical simulation was done by Ayyar *et al.*, (2008) also shown that the clustering of particulates reduces the strength of cast composites. The homogeneity of particulates in the cast is influenced to a great extent by the shear rate, mixing speed and mixing time during the casting process (Tong *et al.*, 2017; Neher *et al.*, 2007). The introduction of particulate powder into the semi-solid state of the matrix material during mechanical stirring can improve the distribution of particulates inside the cast composite. The difference in density between the particulates and matrix material may cause settling of particulates when solidification occurs. The dendritic growth of microstructure during solidification may lead to lowering of the mechanical properties of the composite. Barman *et al.* (2009) manufactured aluminium alloy by stirring the semi-solid material using an electromagnetic field to avoid the formation of dendritic growth.

Measurement of fluid flow characteristics is difficult in a melt-metal system. By this reason, several numerical simulations have been carried out for studying the mixing features in the stir casting with the help of CFD tools. Neher *et al.* (2007) conducted room temperature analogue fluid simulations for PMMC casting for studying the SiC particulate distribution in stir casting. The flow pattern inside the mixing vessel which influences the efficiency of mixing was also observed by CFD simulation (Hashim *et al.*, 2002). Montante and Magelli, (2005) investigated the distribution of solid particles in the liquid inside a stirred vessel using the CFD techniques. The particulate phase and the continuous matrix phase are modelled using the multiphase modelling approach. The governing equations for continuity and momentum of both primary fluid phase and secondary particulate phase are solved in each cell of the domain. The flow patterns can be studied using CFD simulation for arriving at the flow parameters for the better uniformity of particulates.

The Al-SiC PMMC is commonly produced using the stir casting process. The impeller which is immersed in the molten aluminium is rotated about a single axis. The difficulty of getting a homogeneous mixture of particulates is a great task in stir casting method. A new manufacturing method is proposed in this work for getting more uniform particulate distribution in the cast composite. To improve the mixing in the proposed gyro casting mixing system, the mixing cylinder rotates about two mutually perpendicular axes. In this work, the CFD simulation model is developed for gyro casting and validated it with the Power Number obtained from the experiment.

2. METHODS

The proposed system of mixing particulates with fluids, CFD simulations and experiments are discussed in this section.

2.1 Mixing System

The schematic of the stir casting device is as shown in Fig. 1(a) in which the stirrer was rotating about an axis is used for mixing molten aluminium and SiC particulates. The schematic of the gyro casting device is as shown in Fig. 1(b) in which the mixing vessel is rotating about two axes. The axes of rotation of the mixing cylinder for gyro casting mixing are shown in Fig. 1(b). A gyro shaker, commonly used for mixing paints, is used for conducting the experiments for validating the CFD simulation model. The dual axis rotation of the mixing vessel is attained by an induction motor of 1hp. The speed of the induction motor is controlled using an autotransformer to get desired gyration speed between 135 rpm and 180 rpm. The mixing vessel made of transparent acrylic pipe has its height and diameter both kept at 140 mm. For the mixing of viscous fluids in gyro shaker, the spin speed (NS) of the cylinder is set twice as that of gyration speed (NG). Gyro Shaker machines are commonly used for mixing paints; in the spin speed is kept twice than that of gyration speed. The same configuration is used for this experiment also.

2.2 Characteristic Velocity and Power Number

The Reynolds number (R_e) and Power number (N_P) are the commonly used non-dimensional numbers for understanding the performance of mixing in stirred vessels. The validity of CFD simulation model for the stirred vessel is assessed according to the Power number obtained from experiment (Zadghaffari *et al.*, 2010; Deglon and Meyer, 2006; Shekhar and Jayanti, 2002). The characteristic velocity in a mixing system is the ratio of impeller tip velocity to π. The impeller tip velocity is the

maximum velocity of the fluid inside the mixing vessel. Using similar maximum fluid velocity conditions in a gyro shaker mixer, the equation for Characteristic Velocity (U_{ch}) is obtained as;

$$U_{ch} \text{ of gyro shaker } = (N_S D + N_G L) \quad (1)$$

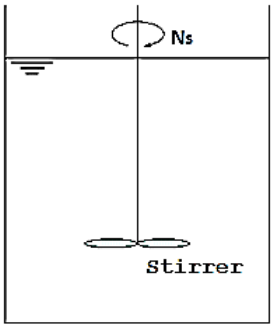

(a) Stir casting

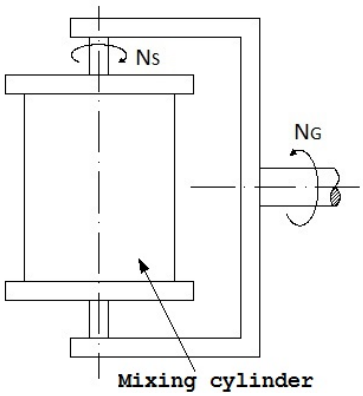

(b) Gyro casting

Fig. 1. Schematics of mixing systems.

where N_S is the spin speed, N_G is the gyration speed, D is the diameter of the mixing tank and L is the height of liquid level.

The power consumption for the mixing, which is known as Mixing Power (P) has to be obtained from the CFD simulation. The mixing power is obtained by integrating the viscous dissipation energy, (Φv) over the entire mixing domain (Alliet-Gaubert *et al.* 2006).

$$P = \iiint_V \mu \, \Phi v \, dV \quad (2)$$

$$\Phi v = 2\left[\left(\frac{dV_x}{dx}\right)^2 + \left(\frac{dV_y}{dy}\right)^2 + \left(\frac{dV_z}{dz}\right)^2\right] + \left[\frac{dV_x}{dy} + \frac{dV_y}{dx}\right]^2 + \left[\frac{dV_x}{dz} + \frac{dV_z}{dx}\right]^2 + \left[\frac{dV_y}{dz} + \frac{dV_z}{dy}\right]^2 \quad (3)$$

where μ is the apparent fluid viscosity and v is the velocity.

The efficiency of a mixing system is defined by the Power number which is a function of the mixing vessel geometry and properties of the liquid phase. The Power number and Reynolds number based on characteristic velocity for a planetary mixing system having two axes rotation as reported by Delaplace *et al.*, (2007) is used in CFD simulation. The equations for Power number and Reynolds number are:

$$N_{PM} = \frac{P}{\rho \, u_{ch}^3 \, L^2} \quad (4)$$

$$R_{eM} = \frac{\rho \, u_{ch} \, D}{\mu} \quad (5)$$

where ρ is the density of liquid phase, N_{PM} is the power number based on characteristic velocity and R_{eM} is the Reynolds number based on characteristic velocity.

2.3 Mixing Time and Mixing Index

The mixing time is the time interval between the segregated state of the liquid and particulate phase to attain a given degree of homogeneity. The Mixing Index (MI) proposed by Rose and Robinson (Huang and Kuo, 2014) as shown in equation 6 is used for assessing the mixing time. Both σ and σ_0 in the equation are standard deviations of the volume fraction of secondary particulate phase at sampling points inside the mixing domain at the current time and initial time. In the presented CFD simulation for comparing the mixing effectiveness, all the cell centre values of the volume fraction of SiC particulates inside the domain are taken as sampling points. As usually taken in stirred vessels, the dispersion time (θ_{99}) is considered as the mixing time when Mixing Index (MI) proposed by Rose and Robinson reaches 0.99 (Javed *et al.*, 2006).

$$\text{Mixing index} = 1 - (\sigma/\sigma_0) \quad (6)$$

2.4 CFD Simulation

CFD solvers use the Finite Volume Method in which the domain under consideration is divided into a finite set of control volumes. The flow field is obtained by solving the conservation equations of the flow such as mass, momentum, energy and species etc. Eulerian k-Ɛ dispersed turbulence model which is a multi-phase model is used for solving the governing equations of the flow.

2.4.1 Governing Equations

The governing equations for the primary liquid phase and secondary granular phase are the following (Zhao *et al.*, 2014; Fletcher and Brown, 2008; Montante and Magelli, 2005).

The continuity equation is:

$$\frac{\partial}{\partial t}(\alpha_l \rho_l) + \nabla.(\alpha_l \rho_l v_l) = 0 \quad \text{and} \quad (7)$$

$$\frac{\partial}{\partial t}(\alpha_s \rho_s) + \nabla.(\alpha_s \rho_s v_s) = 0 \quad (8)$$

The momentum equation is:

$$\frac{\partial}{\partial t}(\alpha_l \rho_l v_l) + \nabla.(\alpha_l \rho_l v_l v_l) = -\alpha_l \nabla p + \nabla.\bar{\bar{\tau}}_l + \alpha_l \rho_l g + F_l + K_{sl}(v_s - v_l) \quad (9)$$

$$\frac{\partial}{\partial t}(\alpha_s \rho_s v_s) + \nabla.(\alpha_s \rho_s v_s v_s) = -\alpha_s \nabla p + \nabla.\bar{\bar{\tau}}_s + \alpha_s \rho_s g + F_s + K_{ls}(v_l - v_s) \quad (10)$$

where α is the volume fraction, v is the velocity and p is the pressure. The subscripts l and s stand for

liquid primary phase and solid secondary phase respectively, and $\bar{\bar{\tau}}_{l,s}$ is the phase stress-strain tensor which is:

$$\bar{\bar{\tau}}_{l,s} = \alpha_{l,s}\mu_{l,s}\left[\left(\nabla v_{l,s} + \nabla v_{l,s}^{T}\right) - \frac{2}{3}I\nabla.\, v_{l,s}\right] \quad (11)$$

The volume fractions of primary liquid phase and secondary particulate phase are controlled by the equation:

$$\alpha_l + \alpha_s = 1 \quad (12)$$

The momentum exchange coefficient is calculated by Gidaspow model combining with the WEN and YU model and the Ergun equation (Zhao *et al*., 2014; Tamayol *et al*., 2008).

$$K_{ls} = K_{sl} = \frac{3}{4}C_D\frac{\alpha_s\alpha_l\rho_l|v_s - v_l|}{d_s}\alpha_l^{-2.65} \quad (13)$$

$$C_D = \frac{24}{\alpha_l Re_s}[1 + 0.15(\alpha_l Re_s)^{0.687}] \quad (14)$$

$$Re_s = \frac{\rho_l d_s|v_s - v_l|}{\mu_l} \quad (15)$$

Where C_D is the drag coefficient and d_s is the diameter of the secondary particulate phase.

2.4.2 Turbulence Modeling

Since the fluid flow inside the mixing vessel is highly swirling, the RNG k-Ɛ turbulence flow model which produces better results is chosen for solving the turbulence quantities (Hreiz *et al*., 2011; Taghvi *et al*., 2011; Wang *et al*., 2010; Razmi *et al*., 2009). Effect of swirl on turbulence for improving the accuracy of flow behaviour is included in this model. The governing equations for turbulent kinetic energy (k) and turbulent energy dissipation rate (Ɛ) are given in equation 16 and 17 (Wang *et al*., 2010; Tamayol *et al*., 2008).

$$\frac{\partial}{\partial t}(\rho k) + \frac{\partial}{\partial x_i}(\rho k u_i) =$$

$$\frac{\partial}{\partial x_j}\left(\alpha_k\mu_t\frac{\partial k}{\partial x_j}\right) - \rho\overline{u_i'u_j'}\frac{\partial u_j}{\partial x_i} - \quad \rho\varepsilon \quad (16)$$

$$\frac{\partial}{\partial t}(\rho\varepsilon) + \frac{\partial}{\partial x_i}(\rho\varepsilon u_i) = \frac{\partial}{\partial x_j}\left(\alpha_\varepsilon\mu_t\frac{\partial \varepsilon}{\partial x_j}\right) -$$

$$C_{1\varepsilon}\frac{\varepsilon}{k}\rho\overline{u_i'u_j'}\frac{\partial u_j}{\partial x_i} - C_{2\varepsilon}\rho\frac{\varepsilon^2}{k} - R_\varepsilon \quad (17)$$

The effective viscosity (μ_t) by considering the effect of swirl is:

$$\mu_t = \rho C_\mu\frac{k^2}{\varepsilon}f\left(\alpha_s, \Omega, \frac{k}{\varepsilon}\right) \quad (18)$$

$$R_\varepsilon = \frac{C_\mu\rho\eta^3(1-\eta/\eta_0)}{1+\beta\eta^3}\frac{\varepsilon^2}{k} \quad (19)$$

The closure coefficients are, α_k=1.393, α_ε=1.393, C_μ=0.0845, α_s=0.07, η_0=4.38 and β=0.012.

$\eta = Sk/\varepsilon$, where, S is the modulus of the mean rate-of-strain tensor and is given by

$S = \left(2S_{ij}S_{ij}\right)^{\frac{1}{2}}$ where S_{ij} is the rate-of-strain tensor

$$S_{ij} = \frac{1}{2}\left(\frac{\partial\bar{u}_i}{\partial x_j} + \frac{\partial\bar{u}_j}{\partial x_i}\right) \quad (20)$$

where Ω is the characteristic swirl number, and $C_{1\varepsilon}$=1.42 and $C_{2\varepsilon}$=1.68 are the model constants.

The effect of mass transfer due to cavitation, virtual mass force, lift force, evaporation-condensation and boiling are not considered. A Finite volume based CFD code in Fluent 16.0 module of ANSYS software is used for solving the governing equations of the fluid flow. Two sets of CFD simulations are carried out. The first set of simulation is for developing gyro shaker CFD model by validating with experimental. The second set of simulation is carried out for comparing the mixing performance of gyro casting with the simulation for stir casting carried by Neher *et al*., (2007). No-slip boundary condition is applied to the closed rotating walls so that the velocity of the fluid stuck on the walls has the same as that of the velocity of the walls.

2.5 Experiment for Mixing Power

In order to validate the CFD simulation, an experiment was conducted to arrive at the power number of the gyro shaker. Experimental setup for obtaining mixing power is shown in Fig. 2. Twenty percent of the total volume of mixing cylinder at the bottom of the tank was filled with SiC of 30 µm size and the rest was filled with glycerol. Viscosity of glycerol at a room temperature of 34^0 C was measured using Brookfield DV 2T Extra Viscometer was found to be 0.4659 PaS. Density Meter DMA 35 Anton Paar instrument was used for measuring the density of glycerol and was found to be 1259 kg/m^3. The density of SiC was considered as 3200 kg/m^3. The maximum and minimum gyration speeds of the gyro shaker machine were 180 rpm and 135 rpm respectively. The mixing power was measured at five different gyration speeds which were obtained by adjusting the speed regulator. Power and current was measured using PX110 Power meter – Metrix instrument. The field resistance (R) of the motor was measured and found to be 2Ω.

The mixing power was calculated by taking the difference in power consumed by the motor at load and no load conditions. Frictional power was assumed to be independent on speed and equation (21) is used for obtaining the mixing power.

$$P_{md} = P_w - I^2 R \quad (21)$$

where P_{md} is power consumed by mixing the ingredients, P_w is power meter reading and I is the current drawn by the motor.

For validating the simulation model with experiment, SiC particulates of 30-micron size and 20% volume fraction with glycerol was used. The computational domain was a cylinder having diameter and length equal to 140 mm. No-slip boundary condition was applied to the walls of the vessel. The SIMPLE (Semi-Implicit Method for Pressure-Linked Equations) pressure-velocity coupling, a second-order upwind scheme for spatial derivatives, least squares cell-based gradient formulation, and QUICK (Quadratic Upwind Interpolation for Convective Kinetics) volume fraction parameter was used. The time step size was set to 0.001 sec and the Spin speed was set as twice as that of Gyration speed as set in a gyro shaker machine.

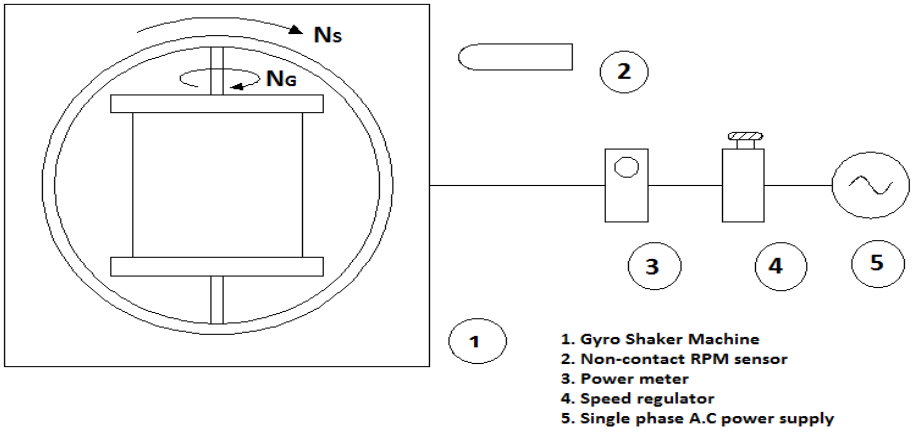

Fig. 2. Experimental setup.

2.6 Gyro Casting Simulation

Neher *et al*., (2007) conducted an experimental study on mixing of SiC particulates in liquids with two different viscosity levels for examining the effect of viscosity of liquids in dispersion time. The particle size and speed of stirring were also varied during the experiment. CFD simulation was also conducted to determine the steady-state particulate distribution in the stir casting of liquid aluminium and mushy state aluminium with 10% SiC of 13 µm size. The experiment and simulation were conducted by replacing liquid aluminium with water having an almost same viscosity of 1 mPaS. Similarly, the mushy state aluminium was replaced by glycerol having almost the same viscosity of 300 mPaS. The computational domain of the stirred vessel was a crucible of 105 mm diameter and was filled with liquid at the height of 65 mm. The stirrer was made of steel having four blades with a diameter of 80 mm. In this paper, the dispersion time and particulate distributions obtained from the CFD simulation model of gyro casting was compared with the values obtained from the works conducted by Neher *et al*., (2007).

The simulation for comparing the effectiveness of the mixing system with stir casting was carried out in laminar model for glycerol/water system and k-Ɛ turbulent model in water system as the simulations conducted by Neher *et al*., (2007). The computational domain for gyro casting was a cylinder having equal diameter and length of 90 mm so as get the same volume of domain in the stir casting. The SiC particulate size is 13 microns and volume fraction is 10%. The Spin speed was taken as twice than that of Gyration speed. CFD simulation is carried out with values of spin speed and gyration speed selected such a way that the characteristic velocity is same as that of the values in the experiment conducted by Neher *et al*., (2007).

3. RESULTS AND DISCUSSION

3.1 VALIDATION OF THE SIMULATION MODEL

Validation for checking the credibility of simulation model was done by comparing the mixing power obtained from the experiment with the simulation results. The power consumed for the mixing was found at different gyration speeds of the mixing vessel. CFD simulations were completed for the different gyration speeds and mixing power was determined using viscous dissipation method.

A grid independence study was carried out using Richardson's extrapolation method (Balduzzi *et al*., 2016; Wahba, 2013) for the simulation model developed for comparing with the experimental results. The CFD simulation was carried out for three domains of polyhedral cells with a grid refinement factor of 1.37. Tetrahedral cells of 619899, 223734 and 91436 numbers converted to polyhedral cells of 108859, 42657 and 16707 numbers for obtaining a monotonic convergence of the flow parameters. The Mixing Power was obtained by extrapolating the values determined from the three simulation models. The GCI (Grid Convergence Index) values for mixing power, volume weighted average pressure and the volume weighted average velocity were less than 5%. So, it was concluded that the CFD simulation is grid independent

3.2 Power Characteristics of the Gyro Shaker

Mixing power for different gyration speeds as obtained from experiment and CFD simulation are shown Fig. 3. Mixing power was found to be increasing almost linearly for both experiment and simulation. The maximum deviation was found to be 8% at a gyration speed of 176.8 rpm. Power number for Reynolds numbers based on characteristic velocity is shown in Fig. 4. The power number was found to be slightly decreasing as the gyration speed increases for both experiment and simulation model.

3.3 Mixing Performance Evaluation

Mixing performance of the developed CFD simulation model of gyro casting was compared with the CFD simulation model developed for stir casting by Neher *et al*., (2007) to mix SiC particulates with water and glycerol/water solution.

The computational domain for comparing the mixing performance was designed for the same quantity of liquid phase and particulate phase taken in the stir casting. Both the diameter and height of the cylindrical mixing vessel were 90 mm. The gyration speed of the mixing vessel was set so as to get the same characteristic velocity of stir casting.

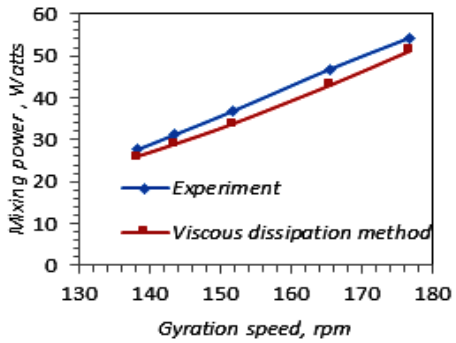

Fig. 3. Power characteristics of the gyro shaker.

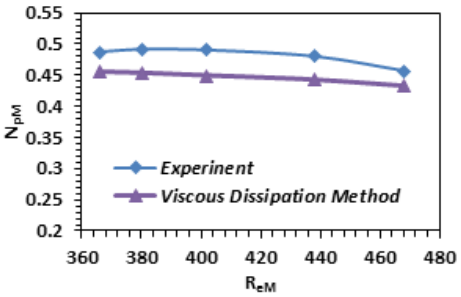

Fig. 4. Power Number variation with respect to Reynolds number based on the Characteristic velocity of the gyro shaker.

The grid independence study was carried out for both the simulation models developed for water and glycerol/water systems for comparing with the stir casting results. The CFD simulation was carried out for three domains of polyhedral cells with a grid refinement factor of 1.39. Tetrahedral cells of 632495, 231057 and 84085 numbers are converted to polyhedral cells of 111055, 41336 and 15497 numbers for obtaining a monotonic convergence of the flow parameters. The Grid Convergence Index (GCI) for mixing power, volume weighted average pressure and volume weighted average velocity were obtained for the above flow parameters were less than 5%. So, it is concluded that the CFD simulation is grid independent.

3.3.1 Mixing Time Evaluation from CFD Simulation

Mixing time for the water system for both stir casting and gyro casting are tabulated in Table 1. The mixing time was high at 200 rpm in stir casting which indicates the stirrer speed is very much close to the just-suspension speed. The mixing time was almost same for 200 rpm, 250 rpm and 300 rpm for stir casting. In stir casting, the mixing was achieved by the rotation of the impeller. Far regions from the impeller get mixed slowly. When the speed was increased, the centrifugal action threw away the particulates at a higher rate against the viscous resistance offered by the fluid resulting a better mixing. Mixing time for gyro shaker was found to be decreasing as the speed was increased but slightly increased at a gyration speed of 87.27 rpm which is due to the low recirculation of the particulates through the centre of the mixing tank.

Table 1 Time to achieve uniform distribution of SiC particulates in the water system

Neher *et al.* stirring speed (rpm)	Gyration speed (rpm)	Mixing time, θ99 (Sec)	Neher *et al.*, (2007) dispersion time (Sec)
100	29.63	61.84	170
200	58.18	43.44	16
250	72.73	26.85	15
300	87.27	27.24	14

Table 2 Time to achieve uniform distribution of SiC particulates in glycerol/water system

Neher *et al.* stirring speed (rpm)	Gyration speed (rpm)	Mixing time, θ_{99}(Sec)	Neher *et al.*, (2007). dispersion time (Sec)
200	58.18	26.34	2335
300	87.27	15.97	1030
400	116.36	9.80	720
500	145.45	6.26	540

Mixing time for both stir casting and gyro casting for the glycerol/water system are tabulated in Table 2. Mixing time in stir casting was found to be much higher than that of the gyro casting. The viscous resistance offered by the fluid is more in this glycerol/water system than the water system. Fluid near the stirrer will mix more and the movement of the particulates towards the far regions is constrained by the high viscous resistance offered by the fluid in stir casting. The mixing time for glycerol/water system was found to be low in case of gyro casting as compared to that of stir casting. It was also lower than water system of gyro casting. Besides, the centrifugal action created by the high viscous fluid inside the rotating vessel of gyro casting device produces better recirculation of fluid.

3.3.2 Distribution of SiC Particulates

The contours of volume fraction inside the mixing vessel before the commencement of mixing is shown in Fig. 5. The SiC particulates of 10 vol.% of the total domain were patched before the beginning of the transient simulation. The contours of the volume fraction of the SiC particulate at the middle

of the vertical section for water system at 40 seconds, 50 seconds and 60 seconds after the commencement of mixing are shown in Fig. 6. For glycerol/water system the same is shown as in Fig. 7 after 10 seconds, 20 seconds and 30 seconds after the commencement of mixing. As the speed was increased, the rate of mixing also increased. A non-uniformity of particulate distribution was found near the centre of the mixing tank at lower gyration speed in both systems. The increased rate of mixing in glycerol/water system is due to the high viscosity of the glycerol/water solution. It is clear from the volume fraction contours that the mixing near the centre of the tank is very slow compared to the area near the walls.

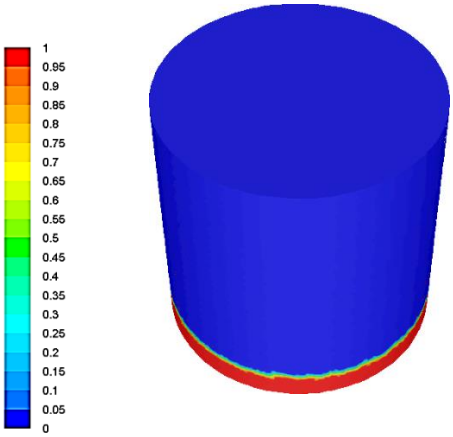

Fig. 5. Contours of volume fraction before the commencement of mixing.

The distribution of SiC particulates in the water system at various locations and different equivalent stirrer speeds at 40 seconds, 50 seconds and 60 seconds after the commencement of mixing along with the steady-state simulation are shown in Fig. 8, 9, 10 &11. The steady state distribution of SiC particulate obtained from the simulation conducted by Neher *et al*., (2007) is also plotted in these graphs for comparing with stir casting. The various radial distances along the central axis of the mixing vessel P, Q, S and T are taken from the bottom of the tank at height ratio of 0, 0.108, 0.538 and 0.769 respectively. The positions of P, Q, S and T represent the bottom wall, bottom region, middle region and top regions of the mixing vessel respectively. For a perfect homogenous suspension of particulates, the volume fraction of the SiC particulate should be 0.1 everywhere inside the fluid domain. At lower speeds, the time taken to get a uniform distribution is found more in the water system for gyro casting. At lower speeds, there was an accumulation of SiC particulates near the centre of the bottom wall in the water system for stir casting. The SiC particulate distribution at the lower region of the mixing vessel was found to be more uniform at higher speeds in gyro casting. Even though there was some degree of non-uniformity in the distribution of SiC particulates in the middle and upper regions of the mixing vessel, the particulate distribution was better in the water system which describes the mixing SiC particulates with liquid aluminium.

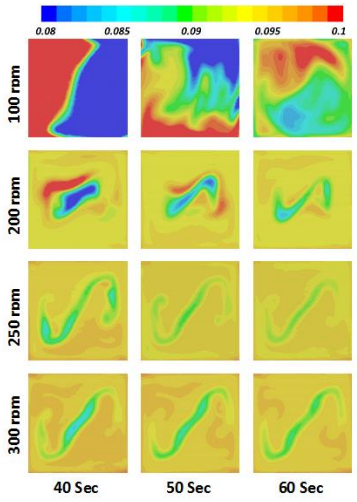

Fig. 6. Contours of the Volume fraction of SiC in the Water system.

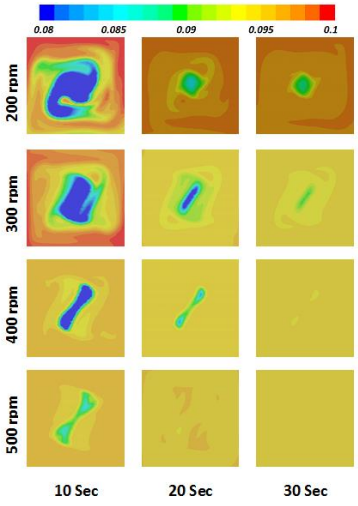

Fig. 7. Contours of the Volume fraction of SiC in glycerol/water system.

The particulate distribution for glycerol/water system after 10 seconds, 20 seconds and 30 seconds and steady state are as plotted in Fig. 12, 13, 14 & 15. These figures show that the mixing rate is more in the glycerol/water system. The SiC particulate distribution was found to be more uniform in glycerol/water system for gyro casting. The momentum transfer is more in glycerol/water system than water system. The intermolecular forces are strong in highly viscous fluids. The higher viscosity of the glycerol/water system provided better mixing in case of gyro casting than stir casting. The accumulation of particulates near the centre of the tank was obtained at lower speeds in the stir casting. The fluctuation in concentration level of particulates inside the mixing domain was

found more in stir casting than gyro casting for both water and glycerol/water systems.

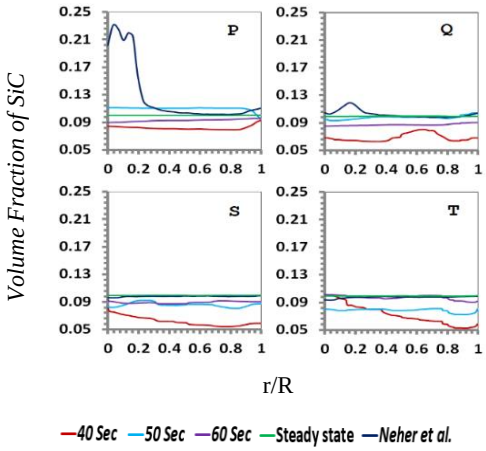

Fig. 8. Distribution of SiC in the water system at an equivalent stirrer speed of 100 rpm.

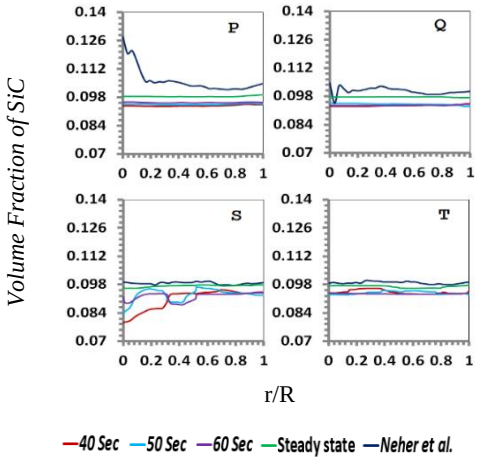

Fig. 9. Distribution of SiC in the water system at an equivalent stirrer speed of 200 rpm.

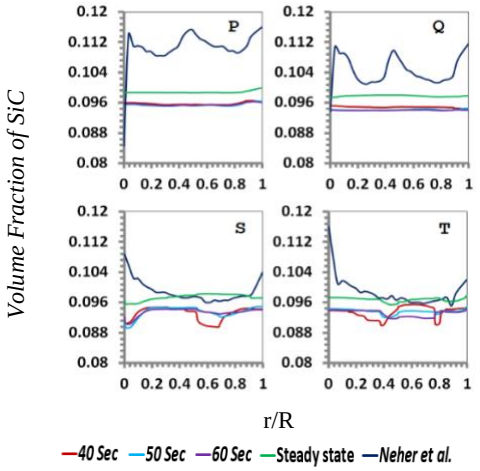

Fig. 10. Distribution of SiC in the water system at an equivalent stirrer speed of 250 rpm.

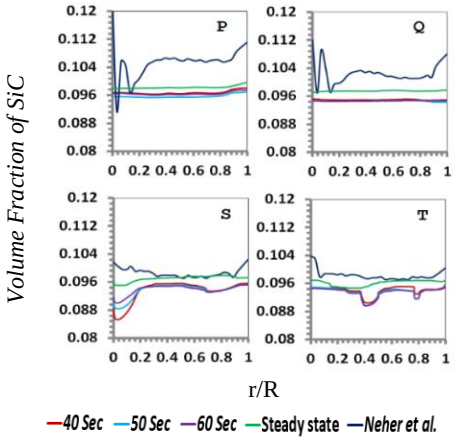

Fig. 11. Distribution of SiC in the water system at an equivalent stirrer speed of 300 rpm.

The contours of the volume fraction of SiC particulates obtained from the steady-state simulation for the water system and glycerol water system are shown in Fig. 16 & 17. The centrifugal force has resulted in transporting particulates as the speed was increased. The strong swirling flow resulted by this centrifugal force drives the solid particles towards the walls of the mixing cylinder. This has resulted in a small amount of increased concentration near the walls of the mixing tank in the water system as it has low viscosity. The difference in volume fraction of the SiC particulates in the glycerol/water system having increased viscosity is negligibly small.

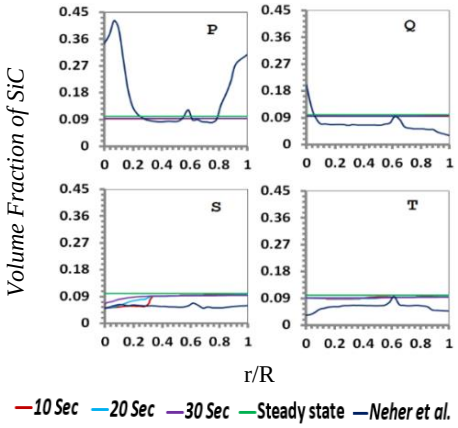

Fig. 12. Distribution of SiC in glycerol/water system at an equivalent stirrer speed of 200 rpm.

3.3.3 Flow Pattern for Gyro Casting

The streamlines of fluid flow, velocity contour and velocity vector for water system at gyration speed of 87.27 rpm obtained from the steady-state simulation is shown in Fig. 18, 20 and 22 respectively. For Glycerol/water system these are shown in Fig. 19, 21 and 23 respectively. The streamlines were plotted in the entire domain whereas the velocity contour and velocity vectors were plotted in the middle vertical section. The mixing was found to be vigorous in both systems.

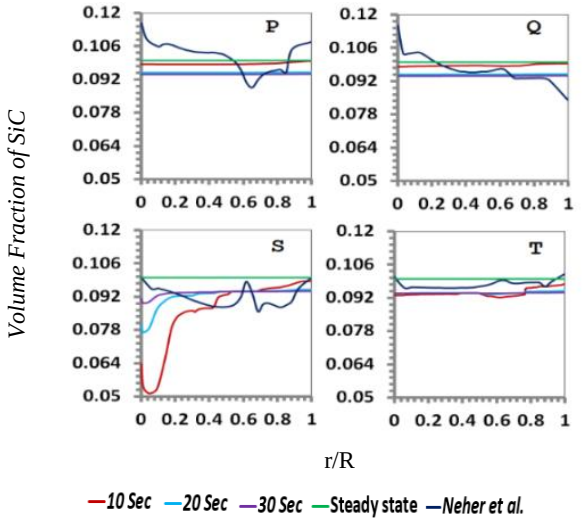

Fig. 13. Distribution of SiC in glycerol/water system at an equivalent stirrer speed of 300 rpm.

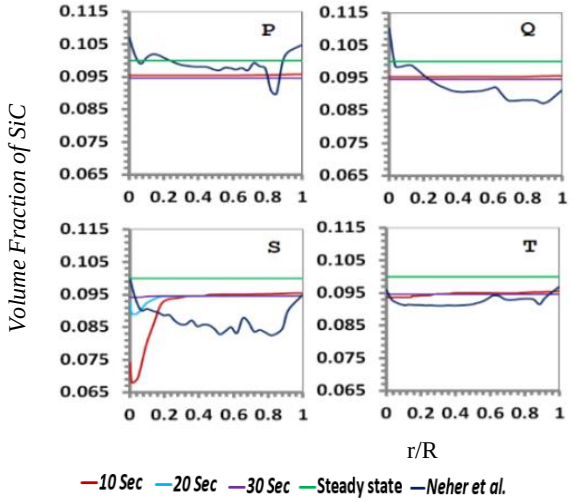

Fig. 14. Distribution of SiC in glycerol/water system at an equivalent stirrer speed of 400 rpm.

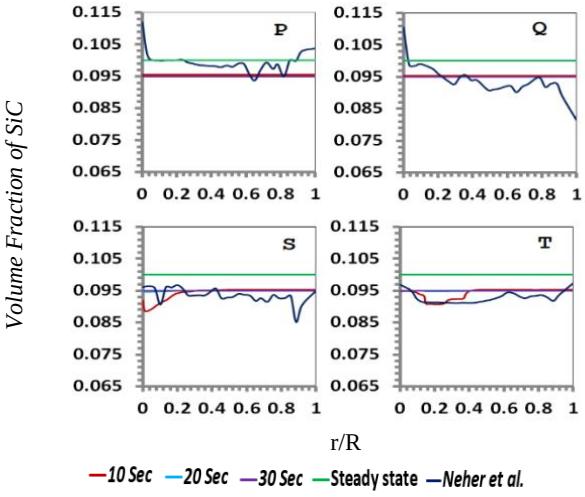

Fig. 15. Distribution of SiC in glycerol/water system at an equivalent stirrer speed of 500 rpm.

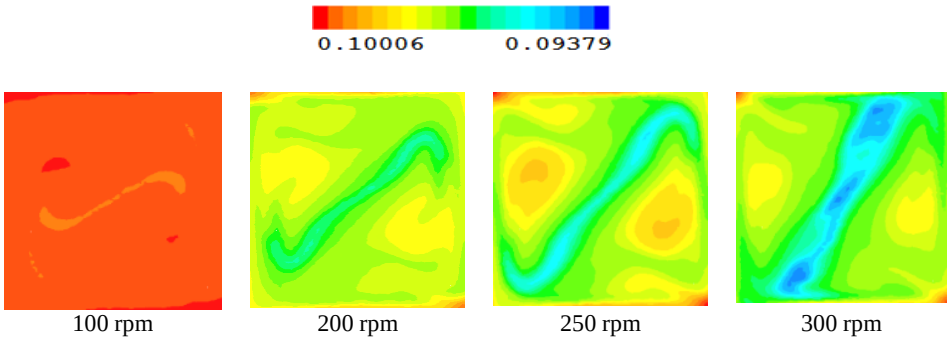

Fig. 16. Contours of the volume fraction of SiC in steady-state simulation for water system.

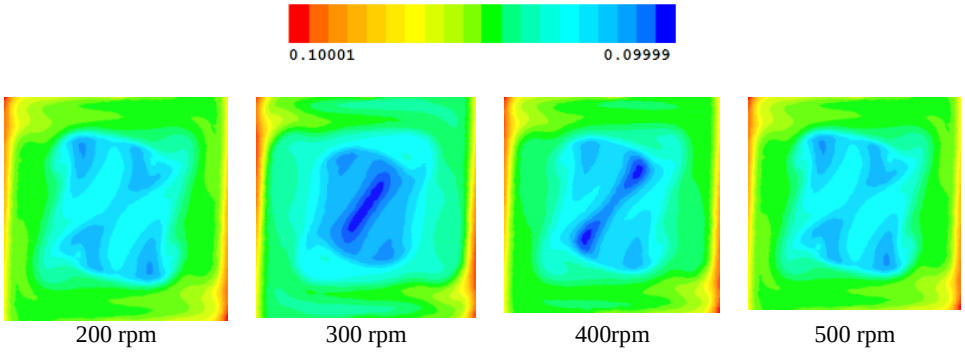

Fig. 17. Contours of the volume fraction of SiC in steady-state simulation for glycerol/water system.

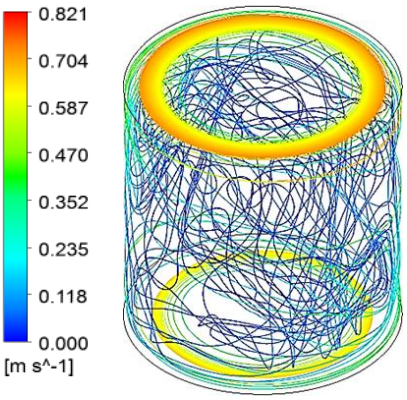

Fig. 18. Streamlines of fluid flow for water system.

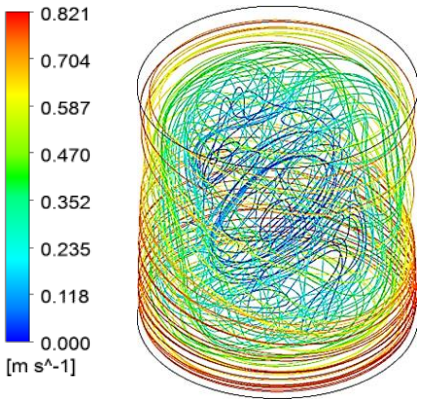

Fig. 19. Streamlines of fluid flow for glycerol/water system.

The flow path is found circulating near the walls of the mixing tank in the water system. The fluid velocity near the centre of the mixing tank was found to be more in glycerol/water system than water system. This is due to the higher viscosity of the glycerol/water system which helps to transfer the momentum delivered by the walls of the mixing tank. The circulation of the flow near the centre of the tank was found from velocity vector plot for glycerol/water system. The circulation of fluid flow for the water system is found to be near the corners of the mixing tank.

4. CONCLUSION

As far as composite materials are concerned; the attainment of a uniform particulate distribution is the foremost deciding factor which ensures good mechanical properties of the casted product. This paper describes the idea of developing a two axes rotation mixing system with the aim of obtaining a uniform particulate distribution in composite materials. CFD simulations were performed to study the effects of mixing SiC particulates with liquid and semi-solid aluminium. Analogue simulations were done by replacing liquid aluminium with water and semi-solid aluminium with glycerol/water mixture.

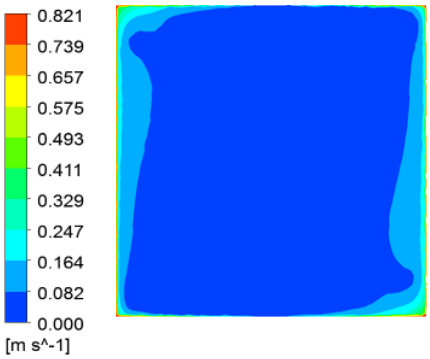

Fig. 20. Velocity contour of the water system.

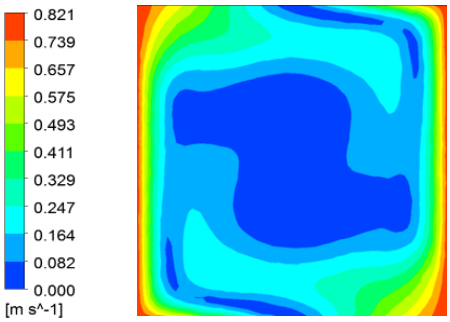

Fig. 21.Velocity contour of glycerol/water system.

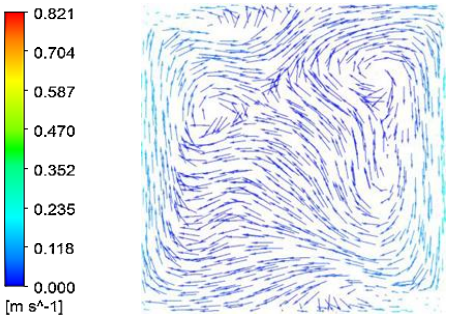

Fig. 22. Velocity vector of the water system.

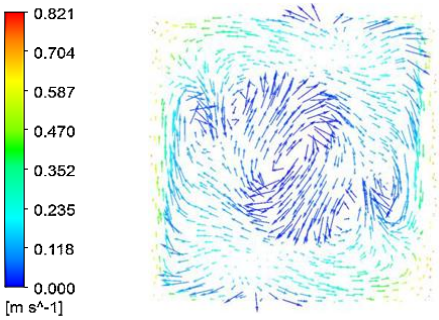

Fig. 23. Velocity vector of glycerol/water system.

The simulation studies for the gyro casting were performed using CFD modelling method, and Eulerian k-Ɛ dispersed multi-phase turbulence model was used. Grid independence study was also conducted to determine the consistency of the flow variables. An experiment was conducted for obtaining mixing power to validate the CFD simulation model. Equivalent viscosity model was used to conduct simulation studies to understand the effects of mixing SiC particulates with the above-mentioned liquid and semi-solid aluminium. The mixing performance of gyro casting was compared with the existing stir casting for the same characteristic velocity of the liquid flow inside the mixing device. It could be concluded the mixing time was found to be less and SiC particulate distribution was more uniform when the gyro casting method was used in place of stir casting.

Hence, it can be concluded that the adoption of the proposed gyro casting method would be more effective in achieving a more homogeneous suspension of particulates in PMMC. Moreover, the change brought about in the mixing process resulted in the alleviation of dendritic growth of microstructures during solidification which would enhance the mechanical properties of the cast composite.

ACKNOWLEDGEMENTS

We would like to acknowledge the University of Calicut and the Department of Mechanical Engineering, Government Engineering College, Thrissur, India for extending the facilities to carry out this study.

REFERENCES

Aigbodion, V. S. (2014). Thermal ageing on the microstructure and mechanical properties of Al-Cu-Mg alloy/bagasse ash particulate composites. *Journal of King Saud University – Engineering Sciences* 26, 144-151.

Alliet-Gaubert, M., R. Sardeing, C. Xuereb, P. Hobbes, B. Letellier and P. Swaels (2006). CFD analysis of industrial multi-staged stirred vessels. *Chemical Engineering and Processing* 45, 415-421.

Ayyar, A., G. A. Crawford, J. J. Williams and N. Chawla (2008). Numerical simulation of the effect of particle spatial distribution and strength on tensile behavior of particle reinforced composites. *Computational Material Science* 44, 496–506.

Balduzzi, F., A. Bianchini, G. Ferrara and L. Ferrari (2016). Dimensionless numbers for the assessment of mesh and time step requirements in CFD simulations of Darrieus wind turbines. *Energy* 97, 246-261.

Barman, N., P. Kumar and P. Dutta (2009). Studies on transport phenomena during solidification of an aluminium alloy in the presence of linear electromagnetic stirring. *Journal of Materials Processing Technology* 209, 5912-5923.

Behera, R., N. R. Mohanta and G. Sutradha (2012). Distribution of SiC particulates in stir cast

Aluminium alloy Metal matrix composites and its effect on mechanical properties. *International Journal of Emerging trends in Engineering and Development* 1, 194-205.

Deglon, D. A. and C. J. Meyer (2006). CFD modelling of stirred tanks: Numerical considerations. *Minerals Engineering* 19, 1059-1068.

Delaplace, G., R. K. Thakur, L. Bouvier, C. Andre and C. Torrez (2007). Dimensional analysis for planetary mixer: Mixing time and Reynolds numbers. *Chemical Engineering Science* 62, 1442- 1447.

Ezatpour, H. R., S. A. Sajjadi, M. H. Sabzevar and Y. Huang (2014). Investigation of microstructure and mechanical properties of Al6061-nanocomposite fabricated by stir casting. *Materials and Design* 55, 921-928.

Fletcher, D. F. and G. J Brown (2009). Numerical simulation of solid suspension via mechanical agitation: effect of the modelling approach, turbulence model and hindered settling drag law. *International Journal of Computational Fluid Dynamics* 23, 173-187.

Ghauri, K. M., A. Ahmad, R. Ahmad, K. M. Din and J. A. Chaudhary (2013). Synthesis and Characterization of Al/SiC Composite Made by Stir Casting Method. *Pakiastan Journal of Engineering and Applied Science* 12, 102-110.

Gupta, N. K., A. K. Tiwari and S. K. Ghosh (2018a). Heat transfer mechanisms in heat pipes using nanofluids – A review. *Experimental Thermal and Fluid Science* 90, 84-100.

Gupta, N. K., A. K. Tiwari and S.K. Ghosh (2018b). Experimental Study of Thermal Performance of Nanofluid-Filled and Nanoparticles-Coated Mesh Wick Heat Pipes. *Journal of Heat Transfer* 140, 1-7.

Hashim, J., L. Looney and M. S. J Hashmi (1999). Metal matrix composites: production by the stir casting method. *Materials Processing Technology* 92, 1-7.

Hashim, J., L. Looney and M. S. J Hashmi (2002). Particle distribution in cast metal matrix composites – Part II. *Journal of Materials Processing Technology* 123, 258-263.

Hreiz, R., C. Gentric and N. Midoux (2011). Numerical investigation of swirling flow in cylindrical cyclones. *Chemical Engineering Research and Design* 89, 2521-2539.

Huang, A. and H. Kuo (2014). Developments in the tools for the investigation of mixing in particulate systems – A review. *Advanced Powder Technology* 25, 163 - 173.

Javed, K. H., T. Mahmud and J. M. Zhu (2006). Numerical simulation of turbulent batch mixing in a vessel agitated by a Rushton turbine. *Chemical Engineering and Processing* 45, 99-112.

Kandpal, B. C., J. Kumar and H. Sing (2017). Fabrication and characterization of Al_2O_3/aluminium alloy 6061 composites fabricated by stir casting. *Materials Today: Proceedings* 4, 2783-2792.

Montante, G. and F. Magelli (2005). Modelling of solids distribution in stirred tanks: analysis of simulation strategies and comparison with experimental data. *International Journal of Computational Fluid Dynamics* 19, 253-262.

Naher, S., D. Brabazon and L. Looney (2007). Computational and experimental analysis of particulate distribution during Al-SiC MMC fabrication. *Composites: Part A* 38, 719-729.

Prabu, S. B., L. Karunamoorthy, S. Kathiresan and B. Mohan (2006). Influence of stirring speed and stirring time on distribution of particles in cast metal matrix composites. *Journal of Material Processing Technology* 171, 268-273.

Razmi, A., B. firoozbadi and G. Ahmadi (2009). Experimental and numerical approach to enlargement of performance of primary settling tanks. *Journal of Applied Fluid Mechanics* 2, 1-12.

Sharma, K., K. K. Saxena and M. Shukla (2012). Effect of Stone-Wales and Vacancy Defects on the Mechanical Behavior of Carbon Nanotubes Using Molecular Dynamics. *Procedia Engineering* 38, 3373-3380.

Sharma, K., K. S. Kaushalyayan and M. Shukla (2015). Pull-out simulations of interfacial properties of amine functionalized multi-walled carbon nanotube epoxy composites. *Computational Materials Science* 99, 232-241.

Sharma, P., S. Sharma and D. Khanduja (2015). A study on microstructure of aluminium matrix composites. *Journal of Asian Ceramic Societies* 3,240-244.

Shekhar, S. M. and S. Jayanti (2002). CFD study of power and mixing time for paddle mixing in unbaffled vessels. *Transactions of the Institution of Chemical Engineers Part A* 80, 482-498.

Taghvi, M., R. Zadghaffari, J. Moghaddas and Y. Moghaddas (2011). Experimental and CFD investigation of power consumption in a dual Ruston turbine stirred tank. *Chemical Engineering Research and Design* 89, 280-290.

Tamayol, A., B. Firoozabadi and G. Ahmadi (2008). Determination of settling tank performance using an Eulerian-Lagrangian method. *Journal of Applied Fluid Mechanics* 1, 43-54.

Tong, M., J. B. Patel, I. Stone, Z. Fan and D. J. Browne (2017). Identification of key liquid metal flow features in the physical conditioning of molten aluminium alloy with high shear processing. *Computational Material Science*

131, 35-45.

Wahba, E. M. (2013). Non-systematic grid refinement procedures for computational fluid dynamics. *Applied Mathematics and Computation* 225, 829-842.

Wang, L., Y. Zhang, X. Li and Y. Zhang (2010). Experimental investigation and CFD simulation of liquid-solid-solid dispersion in a stirred reactor. *Chemical Engineering Science* 65, 5559-5572.

Yigezu, B. S., M. M. Mahapatra and P. K. Jha (2013). Influence of reinforcement type on microstructure, hardness, and tensile properties of an aluminium alloy metal matrix composite. *Journal of Minerals and Materials Characterization and Engineering* 1, 124-130.

Zadghaffari, R., J. S. Mohghaddas and J. Revstedt (2010). Large-eddy simulation of turbulent flow in a stirred tank driven by a Rushton Turbine. *Computers & Fluids* 29, 1183-1190.

Zhao, H., Z. Zhang, T. Zhang, Y. Liu, G. U. Song-qing and C. Zhang (2014). Experimental and CFD studies of solid-liquid slurry tank stirred with an improved Intermig impeller. *Trans. Nonferrous Metals Society of China* 24, 2650-2659.